2022 IEEE International Conference on Robotics and Automation (ICRA)
May 23-27, 2022. Philadelphia, PA, USA

Autonomous Ultrasound Scanning using Bayesian Optimization and Hybrid Force Control

Raghavv Goel*[1], FNU Abhimanyu*[1], Kirtan Patel[2], John Galeotti[1], Howie Choset[1]

***Abstract*— Ultrasound scanning is an imaging technique that aids medical professionals in diagnostics and interventional procedures. However, a trained human-in-the-loop (HITL) with a radiologist is required to perform the scanning procedure. We seek to create a novel ultrasound system that can provide imaging in the absence of a trained radiologist, say for patients in the field who suffered injuries after a natural disaster. One challenge of automating ultrasound scanning involves finding the optimal area to scan and then performing the actual scan. This task requires simultaneously maintaining contact with the surface while moving along it to capture high quality images. In this work, we present an automated Robotic Ultrasound System (RUS) to tackle these challenges. Our approach introduces a Bayesian Optimization framework to guide the probe to multiple points on the unknown surface. Our proposed framework collects the ultrasound images as well as the pose information at every probed point to estimate regions with high vessel density (information map) and the surface contour. Based on the information map and the surface contour, an area of interest is selected for scanning. Furthermore, to scan the proposed region, a novel 6-axis hybrid force-position controller is presented to ensure acoustic coupling. Lastly, we provide experimental results on two different phantom models to corroborate our approach.**

I. Introduction

Ultrasonography has become an important medical imaging modality especially for diagnostics and interventional procedures because of its real-time feedback, portability and radiation-free nature. Ultrasound imaging, thus, has significant advantages over other techniques like Computed Tomography (CT) or Magnetic Resonance Imaging (MRI). Although ultrasound imaging systems have great capabilities, there is a strong dependence on the trained professional's (sonographer) skill. The sonographer needs to find an appropriate area on the patient to scan, thus moving the ultrasound probe within the area of interest, making subtle corrections to the probes pose, and providing safe, significant and accurate forces through the probe to maintain diagnosticable image quality and prevent patient injury. Such skilled workers are not present everywhere. Therefore, to reduce the involvement of experts, the Robotic Ultrasound System (RUS) is introduced. RUS is the fusion of a robotic system and an ultrasound station with its scanning probe attached to the robot end-effector as shown in Fig. 1. Robotic ultrasound scanning also improves accuracy, stability, repeatability and maneuverability in terms of ultrasound image acquisition. In recent years, a lot of research has been put into improving the autonomy of the RUS [1]–[3], [4]–[6]. But most of these mentioned systems are tele-operated and assistive with a human still required to navigate the US probe to the region of interest.

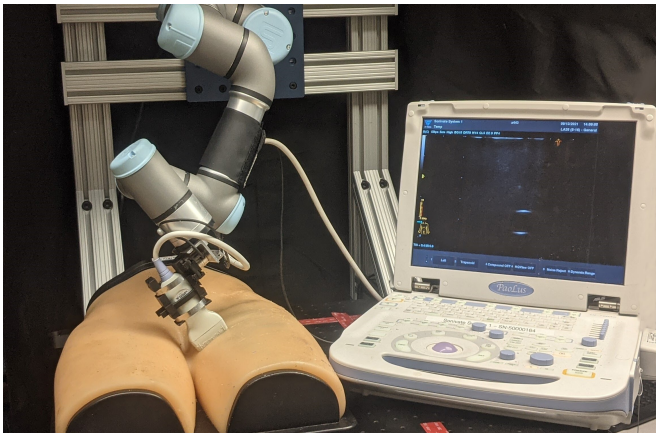

Fig. 1: A Robotic Ultrasound System (RUS), which consists of a 6-DoF UR3e serial manipulator and an ultrasound probe mounted to the robot end-effector.

We propose an autonomous 6-DoF RUS for ultrasound scanning without additional sensor modalities. We use Bayesian Optimization to determine regions with high vessel density in order to narrow down the area to be scanned, eliminating the need to thoroughly scan the entire region. As arteries and veins move along the body in a non-trivial way, traditional function approximation techniques fail to model a good approximation especially with limited number of samples. Bayesian Optimization [7]–[9] not only helps in estimating a function which maps points on the unknown epidermis surface to a reward-like value but also governs where to search on the unknown surface by balancing between exploration and exploitation.

Once the function estimate and the surface contour (using probed points stored) are computed, a reference trajectory over the region with high reward values is created. This reference trajectory is then tracked with a Spherical Linear Interpolation (SLERP) controller and corrected at every instance using noisy force feedback readings (similar to a kalman filter). This approach helps in keeping a balance between the approximated reference trajectory and force readings to ensure proper acoustic coupling. To the best of our knowledge, this is the first work which uses Bayesian Optimization to estimate the vessel density on an unknown

This work was supported by DoD BAA W811XMH-18-SB-AA1 BA180061 and W81XWH-19-C-0101

* Authors of Equal Contribution

[1] are from the Robotics Institute, School of Computer Science, Carnegie Mellon University, 5000 Forbes Ave, Pittsburgh 15213, USA {raghavvg,abhiman2,choset}@andrew.cmu.edu

[2] is from Department of Mechanical Engineering, Carnegie Mellon University, 5000 Forbes Ave, Pittsburgh 15213, USA

surface and then combines it with a 6-axis hybrid force-position controller to perform autonomous scanning on high vessel density region.

This paper is organized as follows: Section II describes the background work. Section III explains the experimental setup, the individual components of the RUS and the integrated pipeline for autonomous scanning. Section IV presents and analyses the results on multiple test subjects. Lastly, Section V has the conclusion and future work.

II. Background

A. Gaussian Process Regression

A common method to estimate unknown functions with limited number of samples is Gaussian Process Regression (GPR) [10]. GPR helps find the distribution over the space of continuous functions, thus computing the estimate of an unknown function along with standard deviation on the estimate. GPR works by sampling values of the unknown function at random points and then computing a mean function and standard deviation function which predicts the value and confidence of the value at any given point respectively. The mean and standard deviation computation depends on a covariance or kernel function which computes how correlated two inputs are. For estimating a function $f : \mathcal{X} \to \mathbb{R}$, a set $\{x_1, x_2 \dots x_m\} \in \mathcal{X}$ is taken, on which $\{y_1, y_2, \dots y_m\}$ are sampled where $y_i = f(x_i) + \epsilon_i$, $\epsilon_i \sim \mathcal{N}(0, \sigma)$. Using these sampled points, a mean function and standard deviation function which represents a distribution over the spaces of continuous functions is computed as

$$\mu(x^*) = K(X, x^*)^T K(X, X)^{-1} Y \tag{1}$$

$$\sigma(x^*) = k(x^*, x^*) - K(X, x^*)^T K(X, X)^{-1} K(X, x^*) \tag{2}$$

where x^* is any point in $\mathcal{X}$, $X = [x_1, x_2 \dots x_m]$, $Y = [y_1, y_2 \dots y_m]$. The matrix K depends on the covariance/kernel function defined as $K : \mathcal{X} \times \mathcal{X} \to \mathbb{R}_{\geq 0}$. A commonly used covariance function is the squared-exponential function which is given as

$$k(x_i, x_j) = \sigma_f \exp\Big(\frac{-\|x_i - x_j\|^2}{2l^2}\Big) \tag{3}$$

where x_i, x_j are the inputs, $\sigma_f \in \mathbb{R}_{\geq 0}$ is the variance and $l \in \mathbb{R}_{\geq 0}$ is the length-scale. Large values of σ imply high uncertainty for points not sampled while large values of l imply large correlation between inputs having large Euclidean distance.

$K(X, x^*) = [k(x_1, x^*), k(x_2, x^*), \dots k(x_m.x^*)] \in \mathbb{R}^m$ is a vector of covariance function values between x^* and X (inputs already sampled) and

$$K(X, X) = \begin{bmatrix} k(x_1, x_1) & \dots & k(x_m, x_1) \\ \vdots & \ddots & \vdots \\ k(x_1, x_m) & \dots & k(x_m, x_m) \end{bmatrix} \tag{4}$$

is the covariance matrix $\in \mathbb{R}^{m \times m}$. Finally, using (1), (2), the estimate of f is

$$\hat{f}(x) \sim \mathcal{N}(\mu(x), \sigma(x)) \tag{5}$$

B. Bayesian Optimization

In a similar vein as previous section, to find the maximum of an unknown function which is expensive to evaluate and lacks linearity and convexity (a 'black-box' function), Bayesian Optimization is used as mentioned in [7]. Bayesian optimization (BO) relies on GPR to find the distribution of the function estimate and then uses an acquisition function to compute the next best location to sample from. Please refer [7] to know more about various types of acquisition functions. A common acquisition function used is Expected Improvement (EI) which helps balance between exploration and exploitation and is given as

$$EI(x) = \begin{cases} (\mu(x) - Y^+)\Phi(z) + \sigma(x)\phi(z) & \text{if } \sigma(x) > 0 \\ 0 & \text{if } \sigma(x) = 0 \end{cases} \tag{6}$$

where, $z = \frac{\mu(x) - Y^+}{\sigma(x)}$ if $\sigma(x) > 0$ otherwise 0; $\Phi(z)$ and $\phi(z)$ are the probability density function (PDF) and cumulative density function (CDF) of normal distribution respectively, and Y^+ is the maximum value sampled. The next best location is given by $x_{next} = \text{ argmax }_x EI(x)$.

C. Quaternion Interpolation

In order to find a smooth reference trajectory between two quaternions, we use SLERP given by:

$$\theta = 2\cos^{-1}(q_a \cdot q_b) \tag{7}$$

$$SLERP(q_a, q_b; t) = \frac{q_a \sin(1 - t) + q_b \sin(r)}{\sin(\theta)} \tag{8}$$

where θ is the angle between q_a and q_b, $t \in [0, 1]$ where $t = 0$ (at q_a) and $t = 1$ (at q_b). Using $SLERP$, quaternions between q_a and q_b can be computed as $q_t = SLERP(q_a, q_b; t)$, which is along the great circle arc on the surface of the unit sphere SLERP was performed upon.

D. Robotics Ultrasound Systems (RUS)

RUS can be categorized into teleoperated, collaborative assisting or autonomous systems. Tele-operative [1]–[3] as well as collaborative assisting systems [4]–[6] have improved image acquisition processes and are able to perform ultrasound scanning in remote areas. But these systems still require a human-in-the loop (HITL).To minimize human intervention, many methods have been explored in autonomous ultrasound systems in recent years [11], [12], [13]. Huang et al. [14] demonstrates autonomous scanning of the coronal plane using an external depth sensor. The system is shown to scan and reconstruct non-flat volumes. This method only plans the scanning trajectory based on external surface features, which may not be the case with many interventional procedures. Hennersperger et al. [15] developed a RUS that autonomously generates trajectories based on the points selected by the physician marked in a MRI or CT scan. This system enables autonomy but is dependent on the MRI/CT scans which are expensive and may not be available at all times. Merouche et al. [16] presents an automatic vessel tracking strategy as an alternative to the teach mode, replay

mode. The pipeline was applied to provide 3-D results of the lower limb arteries. The system could calculate the distance between the center of the vessel and the center element of the probe. However, the system performance would heavily depend upon the detection and tracking of the vessels. [17] provides teleoperated RUS system with three modes for operator: float, haptic and automatic, the automatic mode scans along a desired trajectory recorded by human-in-loop unlike proposed work where the desired trajectory is found using bayesian optimization. Lastly, controlling the movement of the US probe has been done using Reinforcement Learning as shown in [18], [19] but but the success on new patients not in training data is low.

III. Approach

Our approach develops an autonomous ultrasound scanning pipeline, which involves estimating regions with high vessel density and then using force based controller to scan the surface. We call the estimate of vessel density on the phantoms as information map and throughout the paper information map and estimate of vessel density are used synonymously.

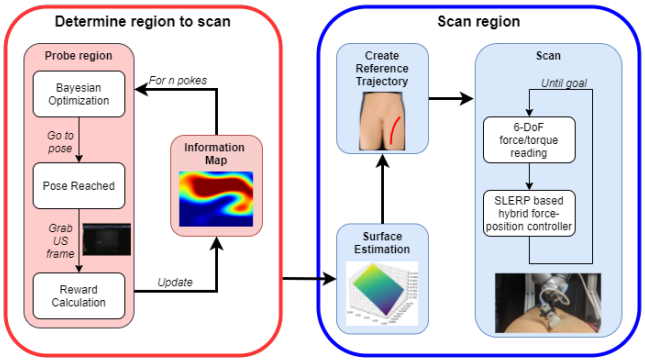

Fig. 2: High-level pipeline depicting the proposed autonomous scanning framework.

A. Experimental setup

We use a Fukuda Denshi portable point-of-care ultrasound scanner (POCUS), with a 5-12 MHz 2D transducer mounted on the Universal Robot UR3e model. The experiments were gathered on two phantoms: a) CAE Blue Phantom anthropomorphic gel model, *blue-gel* shown in Fig. 3(c), and b) CAE Blue Phantom™ Gen II Femoral Vascular Access & Regional Anesthesia Ultrasound Training Model, *leg* as shown in 3(b). The deep learning network for multi-class segmentation was built using TensorFlow [20] and Python. The information map computation using Bayesian Optimization and the force based scanning controller were implemented in Python. Robot Operating System (ROS) was used to combine all of the components together and communicate with the robot. Our work has following assumptions: a) two extreme points are given which essentially tells the bounding-box for our framework to operate on (note that neither depth knowledge along the ultrasound probe is given, nor any knowledge of the surface curvature is known apriori), b) the scan direction is known (usually along the length of the vein/artery). Fig. 3 shows the ee (end-effector) frame which is attached at the end of ultrasound scanner.

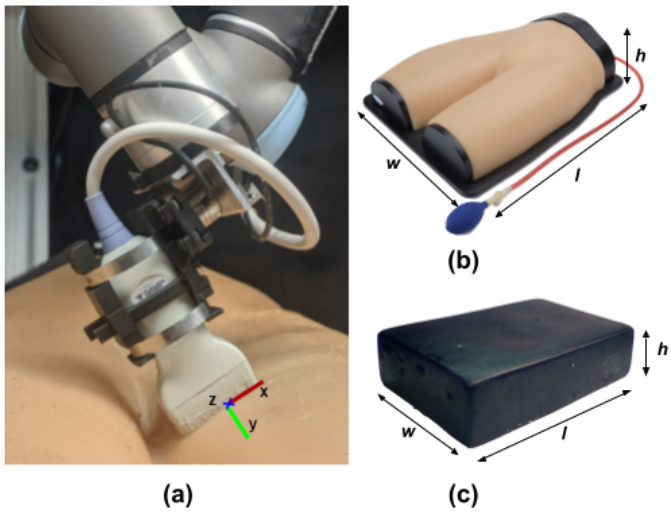

Fig. 3: (a) UR3e robot with the ultrasound probe mounted to the end-effector with the respective tool-frame shown. The ultrasound probe is applying a force normal to the epidermis surface. (b) Leg phantom training model (l = 410mm, w = 340mm, h = 100mm). (c) Blue-gel phantom training model (l = 155mm, w = 95mm, h = 40mm).

B. Estimation using Bayesian Optimization

The input for our Bayesian Optimization is of the form $p = (x, z) \in \mathbb{R}^2$ and the output is $reward \in \mathbb{R}$ which is based on [21], we use both the mean and variance of segmentation to compute the reward by summing the mean value of each pixel in segmented image with a value above a certain threshold and then de-scaling them with variance, the threshold is chosen to be high so that all the dark pixels are filtered out. This is done to prevent inclusion of false-positives. We use the sum of two kernel functions a) k_{SE}: Squared Exponential (or radial basis function) similar to Eq. (3) with the change that $l \in \mathbb{R}^{2\times2}$ is a diagonal matrix to emphasis the anisotropic nature of the operation region and b) k_{white_noise}: white noise kernel, therefore, $k_{total} = k_{SE} + k_{white\_noise}$

$$k_{white\_noise}(x_i, x_j) = \begin{cases} \sigma_{noise} & \text{if } x_i = x_j \\ 0 & \text{if } x_i \neq x_j \end{cases} \quad (9)$$

where, $\sigma_{white} \in \mathbb{R}_{>0}$. The white noise kernel is used to model the noise in segmentation measurements. For the choice of acquisition function we use combination of Expected Improvement as mentioned in Eq. (6) and also maximum of uncertainty which is given by

$$p_{next} = \underset{p}{\text{argmax}}\ \sigma(p)\, \forall p \in \mathcal{X} \quad (10)$$

where, $\sigma(p)$ is from Eq. (2), and p_{next} is the next position to probe at.

In our experiments every fourth point is sampled from uncertainty acquisition function while the rest from EI acquisition function in Eq. (6). When a new position for probing

is computed, the normal force and probe alignment is done using force-feedback controller discussed in Subsection III-C.

Lastly, hyper-parameter tuning is done to better fit (smoothen) the estimate of information map on the limited number of inputs sampled by maximising log-liklihood as shown in [22]. In our case the hyper-parameters are $\theta = [l_1, l_2, \sigma_f, \sigma_{noise}]$

$$\theta^* = \underset{\theta}{\operatorname{argmin}} \; -\log\big(p(Y|X,\theta)\big) \tag{11}$$

where, $p(Y|X,\theta) = \frac{1}{\sqrt{2\pi|K|}} \exp(Y^T K^{-1} Y)$, K is from Eq. (4) and is a function of θ, X, Y are the set of position points probed and rewards respectively, l_1, l_2 is the length-scale along *x-axis* and *z-axis* respectively, σ_f is the standard deviation of k_{SE} and σ_{noise} is the standard deviation of k_{white_noise}. We use L-BFGS algorithm [23] to optimize Eq. (11).

Following this we a) compute a linear trajectory passing through region of high vessel density by fitting a cubic polynomial and b) compute normals corresponding to points in linear trajectory by computing a 3-D estimate of the unknown surface using probed points. Note that together the linear trajectory and normals will be called reference trajectory (sequence of poses) for the US probe to scan along.

C. Force based ultrasound scanning

Two different controllers for scanning the surface are discussed. One uses the surface information (known normals to the surface as mentioned earlier) and the other uses the force measurement to scan the surface. We further discuss a novel method which combines the two approaches for a robust scanning controller. The motivation of having a consistent force along/around the normal of the surface is to maintain proper acoustic coupling during scanning to get useful images. At the same time it is crucial that there's no excess force which may affect or distort the data collected during ultrasound scanning. Without taking care of these conditions the segmentation performance will be disrupted.

1) SLERP based hybrid controller: Based on the reference trajectory presented in Subsection III-B, SLERP based controller is used to track the orientations in the reference trajectory by computing the intermediate orientations to follow using

$$r_t = \frac{d(p_t, p_T)}{d(p_0, p_T)} \tag{12}$$

$$q_t = \frac{q_0 \sin(1 - r_t) + q_T \sin(r_t)}{\sin(\theta_t)} \tag{13}$$

where $\theta_t = 2\cos^{-1}(q_0 \cdot q_T)$, $d(.,.)$ is the Euclidean distance, $P_0 = \{p_0, q_0\}$, $P_t = \{p_t, q_t\}$ and $P_T = \{p_T, q_T\}$ are the starting, instantaneous and final pose of the ultrasound probe. $p_t = [p_t^x, p_t^y, p_t^z]$ is the position and $q_t = [q_t^w, q_t^x, q_t^y, q_t^z]$ is the quaternion with respect to the base frame of the robot.

After computing the quaternions $[q_0, \dots q_{t-1}, q_t, \dots q_T]$ the angular velocity is calculated in the end-effector frame as

$$\delta q_t = q_t^{-1} q_{t+1} \tag{14}$$

$$w_{slerp,t} = quat2euler(\delta q_t)/\Delta t \tag{15}$$

The 3 position/linear axis in the end-effector frame of the robot is controlled using the position controller mentioned in [24].

2) Force based hybrid controller: In this controller, force feedback is used along all axis to control the angle made by the probe on the unknown surface to be normal to the surface, and to control the force exerted along the length of probe (*y-axis* in probe frame) to maintain a desired contact in the y-axis of the probe while scanning. This is done by updating the input linear (v_y) and angular velocities ($w_{\text{FF},x}, w_{\text{FF},z}$) to the robot end-effector as

$$v_{y,t} = -D_y(f_{y,t} - f_{y,d}) \tag{16}$$

$$\omega_{\text{FF}x,t} = -D_x(f_{x,t} - f_{x,d}) \tag{17}$$

$$\omega_{\text{FF}z,t} = -D_z(f_{z,t} - f_{z,d}) \tag{18}$$

where, the subscript '$_{\text{FF}}$' implies force-feedback. D_y, D_x and D_z are positive scalar controller gains. To match the surface normal, the desired forces are set as $f_{x,d} = 0N$, $f_{z,d} = 0N$ and $f_{y,d} = -8N$.

3) Combined SLERP + force controller: SLERP based controller is good at following a given orientation trajectory but fails to adjust for abrupt changes in the orientation. Force based orientation controller is good at adjusting for any on-the-fly change but can be noisy. To counter cons of each method, we combine both of them using a Kalman filter like approach, where the SLERP based controller is part of a trivial process model while the force feedback is part of the measurement model based on Eq. (17), Eq. (18). The innovation/measurement residual is given as

$$\tilde{\omega}_t = \omega_{\text{FF},t} - \omega_{slerp,t} \tag{19}$$

The optimal gain is given as $K_t = (I_3 + R)^{-1}$, where $R \in \mathbb{R}^3$ is the covariance of the observation noise of the force sensor and I_3 is the identity matrix. Using Eq. (19) and K_t, we get the the updated angular velocity as

$$\omega_t = \omega_{slerp,t} + K_t \tilde{\omega}_t \tag{20}$$

Note that the gain K_t can also be kept fixed. Experiments were tried by keeping both a fixed and varying gain. Based on the assumptions mentioned earlier angular velocity along *y-axis* is 0.

D. Autonomous RUS Pipeline

The initial point is chosen as the smaller one of the two extreme points given where the probe samples first, after which the given steps are followed:

1) a) The acquisition function mentioned in Subsection III-B gives the location of the next point to go to.
   b) After the desired contact force with the surface is achieved, the raw ultrasound image is passed to the segmentation network via ROS. The network segments the vessels and calculates the reward for the image as

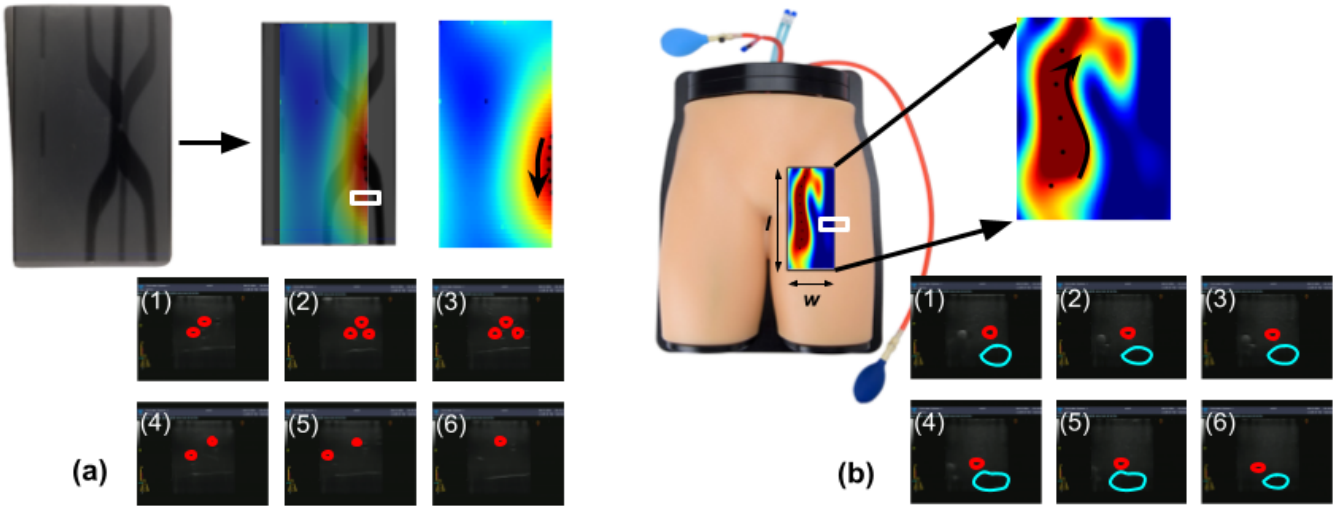

Fig. 4: (a) CT-scan of blue-gel phantom overlayed with its estimate of vessel density by kinematic registration, the scan region is smaller than the actual size of the blue-gel phantom due to width of US probe (shown as a white rectangle). (b) Estimate of vessel density overlayed on left side of the leg phantom (l = 200mm, w = 90mm). Black-dotted line is the scanning trajectory passing along high vessel dense region (red color) for both phantoms. Scanning is performed along black-dotted line, with black arrow showing direction of scanning. Bottom parts of (a) and (b) sub-figures show US images when scanning along the trajectory for both the phantoms.

mentioned earlier. The particular pose along with the obtained reward is saved in a memory buffer.

c) Based on the calculated reward, the hyper-parameters of chosen kernels are updated Eq. (11) and the new estimate of the unknown function is computed based on Eq. (5). After that Step 1.a. is repeated until convergence or maximum iteration is reached.

2) a) Based on the poses of the probed points stored in the memory buffer and the information map, a reference trajectory of poses across high information region is computed.

b) Finally, the designed controller enables the US probe to scan the region of interest. The designed controller uses ROS to command desired trajectory to the robot using the *speedl* command

Note that all the above steps are completed with zero human intervention. A diagram of the system is given in Fig. 2.

IV. Results and Analysis

The experiments are to find the region with the most number of arteries/veins and then to scan this region using the combined SLERP + force feedback controller to get high-quality, densely spaced imaging of the target vessels, which can be used to inform medical decisions and guide clinical actions. For finding regions with high vessel density per ultrasound image frame, we compare between different search strategies of Bayesian optimization. In all the experiments *no knowledge about the phantoms is assumed* except for x, z location of extreme points. Due to the robot arm's limited workspace, experiments were only performed on the left-side femoral region of the leg phantom.

A. Comparing Different Search Strategies

We compare between the following strategies: uncertainty based on Eq. (10), EI based on Eq. (6), a mixture of EI and uncertainty (ours) and finally randomly probing. Information map estimates using all these strategies are shown in Fig. 5 for blue-gel phantom and in Fig. 6 for leg phantom to provide a qualitative comparison and Table I provides a quantitative analysis using two metrics: i) total euclidean distance error (TEDE) between top n points with maximum rewards and ii) zero normalised cross correlation (ZNCC) [25]. These metrics are computed with respect to uniformly probed estimates shown in Fig. 5(a) and Fig. 6(a), which are treated as an approximate ground truth for respective phantoms where red color corresponds to high vessel density regions and the blue color corresponds to low vessel density regions. TEDE compares how well regions with high vessel density are detected in different search strategies with respect to approximate ground truth, and ZNCC compares the whole vessel density estimate of each strategy to the approximate ground truth.

We first tried EI as our search strategy but its exploitation strategy led to overly clustered sampling as shown in Fig. 5(c) and 6(c). The black dots represent the points probed and the majority of them are centred about the maximum information. On the other hand, search based on only uncertainty was too exploratory as shown in Fig. 5(d), 6(d) where the points are spread all over. Therefore, to balance both exploitation and exploration we used a combination of EI and uncertainty to search which is shown in Fig. 5(b), 6(b), here every fourth point was chosen based on uncertainty. Lastly, search was also done using a random strategy, which did not work as well when using a limited number of points for the leg phantom as seen in Fig. 6(e). Due to the small size of the blue-gel phantom, almost all strategies performed similarly when a high number of points were probed. Note that, from Fig. 4(a) the high reward (red-colored) region of information map estimate overlaps with the high vessel density region from the CT-scan. The region with the most vessels in a US frame is where one vessel is bifurcating while

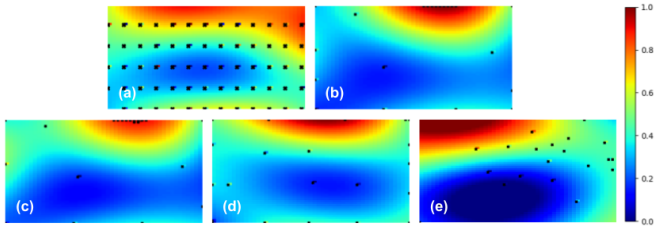

Fig. 5: Blue-gel phantom information map estimates for different search strategies: (a) Uniform (ground truth), (b) Combined EI + uncertainty, (c) EI, (d) Uncertainty, (e) Random. Black-dots are positions where US probe probed. Note that for uniform the number of points were more than the other strategies.

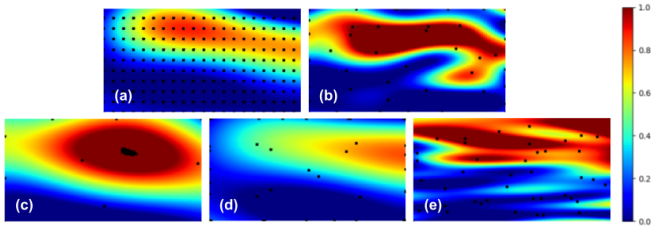

Fig. 6: Leg-phantom information map estimates with the same order of displacement as in Fig. 5

the other passes below it, thus showing 3 vessels (refer to US images in Fig. 4(a)). The images were overlayed using kinematics based registeration. Similarly, Fig. 4(b) shows the scanning for the leg-phantom along high information region, the ultrasound images show the arteries and veins along the scan trajectory. For the leg phantom no ground truth CT-scan was available.

Table I shows that when only 20 points are probed, the TEDE metric gives the best performance with the mixed strategy in both the leg phantom and blue-gel phantom.

B. Comparing Controllers

We compare the quality of the scans obtained using the following controllers: only SLERP, only FF, and combined SLERP + FF (ours). We estimate the quality of the US acquired images using ZNCC. ZNCC measures the quality of the image based on the contact between the probe and the epidermal surface. Note that, the controller tests are only carried on the *leg phantom* as the *blue-gel* is flat as can be seen in Fig. 3(c).

For the given trajectory $[P_0, \dots P_t, \dots P_T]$ as shown in Fig. 4 black-dotted line, we get a ZNCC score of 0.935, 0.933, 0.953 and 0.944 for SLERP, force-feedback (FF), combined SLERP+FF ($K_t = 0.5$) and combined SLERP+FF (varying K_t) respectively, where K_t is from Eq. (20). The upper bound of this metric is 0.993 when the robotic arm is locked in a fixed location with constant force (thus making

TABLE I: Quantitative Comparison of Search Strategies

Experiments	Leg phantom			Blue-gel phantom		
	TEDE		ZNCC	TEDE		ZNCC
	n=20	n=40	n=40	n=20	n=40	n=40
Random	8.32	8.31	0.74	9.11	3.61	0.86
SD	6.67	6.82	0.91	2.99	2.96	0.83
EI	8.42	3.63	0.84	2.43	2.55	0.76
Modified EI	**4.22**	**2.25**	**0.834**	**2.51**	**2.32**	**0.84**

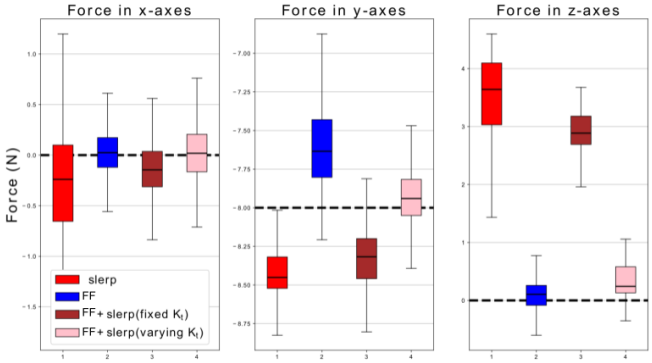

Fig. 7: Force profiles along x, y, z axis of different types of controllers tested on the leg phantom. The black-dotted line shows the desired force.

good contact with the unknown surface as no sweeping being performed which can shake the probe off the normal of the surface) and the lower bound is 0.795 when the robotic arm force constraint is turned off thus leading to jittery contact with the surface.

Apart from the image quality, we also need to ensure proper force profile in all three axes. The desired forces in each direction are $f_{x,d} = 0N$, $f_{z,d} = 0N$ and $f_{y,d} = -8N$. Fig. 7 shows the box-plot of the force in each of the axis for each scanning method. As shown in Fig 7, the combined SLERP + FF (varying K_t) strategy performs the best with mean deviation of $[0.025, 0.31, 0.35]$ and standard deviation of $[0.27, 0.655, 0.261]$ in $[x, y, z]$ on the leg phantom. Comparatively, the SLERP and FF have much higher mean and standard deviation, especially in the x and z direction, because of the approximate nature of the surface reconstruction and the noisy force sensor reading respectively.

The results demonstrate that using our combined control strategy can compensate for errors introduced by the approximate surface reconstruction with force feedback and can also enable smoother scanning, because it is not completely relying on the noisy force sensor.

V. Conclusion and Future Work

This paper presented a solution for an autonomous Robotic Ultrasound System. The autonomy stack was divided in two sections: 1) the Bayesian Optimization based information map estimation and 2) a combined SLERP and force feedback based controller to scan the region with high vessel density extracted from the information map. The pipeline was successfully demonstrated on two medical training phantoms. Furthermore, comparison between different search strategies (acquisition function) for Bayesian Optimization was analyzed. Our force experiments showed that the proposed controller not only gives good quality images but also maintains the desired force profile. For future work, we wish to incorporate the geometry of the ultrasound probe and include the range of forces being applied along the length of the probe by extending Bayesian Optimization to the space of $[x, z, force]$ from $[x, z]$, and improving surface reconstruction by using piece-wise estimation methods.

REFERENCES

[1] J. Wang, C. Peng, Y. Zhao, R. Ye, J. Hong, H. Huang, and L. Chen, "Application of a robotic tele-echography system for covid-19 pneumonia," *Journal of Ultrasound in Medicine*, vol. 40, no. 2, pp. 385–390, 2021.

[2] S. Avgousti, A. S. Panayides, A. P. Jossif, E. G. Christoforou, P. Vieyres, C. Novales, S. Voskarides, and C. S. Pattichis, "Cardiac ultrasonography over 4g wireless networks using a tele-operated robot," *Healthcare technology letters*, vol. 3, no. 3, pp. 212–217, 2016.

[3] K. Arent, M. Cholewiński, W. Domski, M. Drwiega, J. Jakubiak, M. Janiak, B. Kreczmer, A. Kurnicki, B. Stańczyk, D. Szcześniak-Stańczyk *et al.*, "Selected topics in design and application of a robot for remote medical examination with the use of ultrasonography and ascultation from the perspective of the remedi project," *Journal of Automation Mobile Robotics and Intelligent Systems*, vol. 11, no. 2, pp. 82–94, 2017.

[4] M.-A. Janvier, S. Merouche, L. Allard, G. Soulez, and G. Cloutier, "A 3-d ultrasound imaging robotic system to detect and quantify lower limb arterial stenoses: in vivo feasibility," *Ultrasound in medicine & biology*, vol. 40, no. 1, pp. 232–243, 2014.

[5] P. Abolmaesumi, S. E. Salcudean, W.-H. Zhu, M. R. Sirouspour, and S. P. DiMaio, "Image-guided control of a robot for medical ultrasound," *IEEE transactions on robotics and automation*, vol. 18, no. 1, pp. 11–23, 2002.

[6] Z. Jiang, M. Grimm, M. Zhou, J. Esteban, W. Simson, G. Zahnd, and N. Navab, "Automatic normal positioning of robotic ultrasound probe based only on confidence map optimization and force measurement," *IEEE Robotics and Automation Letters*, vol. 5, no. 2, pp. 1342–1349, 2020.

[7] P. I. Frazier, "A tutorial on bayesian optimization," *arXiv preprint arXiv:1807.02811*, 2018.

[8] E. Ayvali, R. A. Srivatsan, L. Wang, R. Roy, N. Simaan, and H. Choset, "Using bayesian optimization to guide probing of a flexible environment for simultaneous registration and stiffness mapping," in *2016 IEEE International Conference on Robotics and Automation (ICRA)*. IEEE, 2016, pp. 931–936.

[9] M. Nishio, M. Nishizawa, O. Sugiyama, R. Kojima, M. Yakami, T. Kuroda, and K. Togashi, "Computer-aided diagnosis of lung nodule using gradient tree boosting and bayesian optimization," *PloS one*, vol. 13, no. 4, p. e0195875, 2018.

[10] C. E. Rasmussen, "Gaussian processes in machine learning," in *Summer school on machine learning*. Springer, 2003, pp. 63–71.

[11] L. Santos and R. Cortesão, "A dynamically consistent hierarchical control architecture for robotic-assisted tele-echography with motion and contact dynamics driven by a 3d time-of-flight camera and a force sensor," in *2015 IEEE International Conference on Robotics and Automation (ICRA)*. IEEE, 2015, pp. 2931–2937.

[12] L.-A. Chanel, F. Nageotte, J. Vappou, J. Luo, L. Cuvillon, and M. de Mathelin, "Robotized high intensity focused ultrasound (hifu) system for treatment of mobile organs using motion tracking by ultrasound imaging: An in vitro study," in *2015 37th Annual International Conference of the IEEE Engineering in Medicine and Biology Society (EMBC)*. IEEE, 2015, pp. 2571–2575.

[13] S. Virga, O. Zettinig, M. Esposito, K. Pfister, B. Frisch, T. Neff, N. Navab, and C. Hennersperger, "Automatic force-compliant robotic ultrasound screening of abdominal aortic aneurysms," in *2016 IEEE/RSJ International Conference on Intelligent Robots and Systems (IROS)*. IEEE, 2016, pp. 508–513.

[14] Q. Huang, J. Lan, and X. Li, "Robotic arm based automatic ultrasound scanning for three-dimensional imaging," *IEEE Transactions on Industrial Informatics*, vol. 15, no. 2, pp. 1173–1182, 2018.

[15] C. Hennersperger, B. Fuerst, S. Virga, O. Zettinig, B. Frisch, T. Neff, and N. Navab, "Towards mri-based autonomous robotic us acquisitions: a first feasibility study," *IEEE transactions on medical imaging*, vol. 36, no. 2, pp. 538–548, 2016.

[16] S. Merouche, L. Allard, E. Montagnon, G. Soulez, P. Bigras, and G. Cloutier, "A robotic ultrasound scanner for automatic vessel tracking and three-dimensional reconstruction of b-mode images," *IEEE transactions on ultrasonics, ferroelectrics, and frequency control*, vol. 63, no. 1, pp. 35–46, 2015.

[17] F. Conti, J. Park, and O. Khatib, "Interface design and control strategies for a robot assisted ultrasonic examination system," in *Experimental Robotics*. Springer, 2014, pp. 97–113.

[18] R. Droste, L. Drukker, A. T. Papageorghiou, and J. A. Noble, "Automatic probe movement guidance for freehand obstetric ultrasound," in *International Conference on Medical Image Computing and Computer-Assisted Intervention*. Springer, 2020, pp. 583–592.

[19] K. Li, J. Wang, Y. Xu, H. Qin, D. Liu, L. Liu, and M. Q.-H. Meng, "Autonomous navigation of an ultrasound probe towards standard scan planes with deep reinforcement learning," in *2021 IEEE International Conference on Robotics and Automation (ICRA)*. IEEE, 2021, pp. 8302–8308.

[20] M. Abadi, A. Agarwal, P. Barham, E. Brevdo, Z. Chen, C. Citro, G. S. Corrado, A. Davis, J. Dean, M. Devin, S. Ghemawat, I. Goodfellow, A. Harp, G. Irving, M. Isard, Y. Jia, R. Jozefowicz, L. Kaiser, M. Kudlur, J. Levenberg, D. Mané, R. Monga, S. Moore, D. Murray, C. Olah, M. Schuster, J. Shlens, B. Steiner, I. Sutskever, K. Talwar, P. Tucker, V. Vanhoucke, V. Vasudevan, F. Viégas, O. Vinyals, P. Warden, M. Wattenberg, M. Wicke, Y. Yu, and X. Zheng, "TensorFlow: Large-scale machine learning on heterogeneous systems," 2015, software available from tensorflow.org. [Online]. Available: https://www.tensorflow.org/

[21] E. Chen, "Towards practical ultrasound ai across real-world patient diversity," Ph.D. dissertation, Carnegie Mellon University Pittsburgh, PA, 2021.

[22] C. E. Rasmussen and C. K. Williams, "Model selection and adaptation of hyperparameters," in *Gaussian processes for machine learning*. MIT Press, 2005, pp. 105–128.

[23] D. C. Liu and J. Nocedal, "On the limited memory bfgs method for large scale optimization," *Mathematical programming*, vol. 45, no. 1, pp. 503–528, 1989.

[24] M. Victorova, D. Navarro-Alarcon, and Y.-P. Zheng, "3d ultrasound imaging of scoliosis with force-sensitive robotic scanning," in *2019 Third IEEE International Conference on Robotic Computing (IRC)*. IEEE, 2019, pp. 262–265.

[25] J. Martin and J. L. Crowley, "Experimental comparison of correlation techniques," in *Int. Conf. on Intelligent Autonomous Systems*. Citeseer, 1995.